Materials Research Proceedings 44 (2024) 70-78 https://doi.org/10.21741/9781644903254-8

Advanced elastic-plastic constitutive models for medium-thickness high-strength steel plates: Microstructure-based parameter identification and verification

HU Xiao[1,a *], ZHOU Yu[2], GAO Chenxin[3], SHI Liya[4], LIAO Yong[4], ZHANG Haiming[3,b *], WANG Feilong[1] and WANG Liangyun[1]

[1]Pangang Group Research Institute Co., Ltd., Panzhihua 617000, China

[2]Pangang Group Panzhihua Steel and Vanadium Co., Ltd., Panzhihua 617000, China

[3]School of Materials Science and Engineering, Shanghai Jiao Tong University, Shanghai, 200240, China

[4]Dongfeng Liuzhou Motor Co., Ltd., Liuzhou 545000, China

[a]yjyhuxiao@pzhsteel.com.cn, [b]hm.zhang@sjtu.edu.cn

Keywords: Constitutive Models, Medium-Thickness Plate, Crystal Plasticity, Yield Criteria, Kinematic Hardening

Abstract. Replacing castings with medium-thickness, high-strength steel sheet (with thickness exceeding 3 mm) stampings can save raw materials and energy, and many medium-thickness plate parts are used in commercial vehicle frame assemblies and cab mounts. However, there are obvious differences between the sheet metal forming mechanisms of medium-thickness plate parts and thin sheet parts. There is a lack of systematic research on the issues of anisotropy, springback, non-uniform material flow, and fracture that exist in the sheet metal forming of medium-thickness plate parts. In this study, we coupled the three-dimensional anisotropic yield criteria Hill 48 and the kinematic hardening models (Armstrong-Frederick) to develop elastic-plastic constitutive models for the forming simulation of medium-thickness high-strength steel plates. Taking the 5-mm-thick 750L high-strength steel as the research object, for the problem that the anisotropic yield criterion parameters (especially in the thickness direction) are difficult to calibrate, we employed high-resolution full-field crystal plasticity simulations to obtain the parameters of the yield criterion, and determined the material parameters of the kinematic hardening models by the inverse analysis method. Through this multiscale modeling technique, we obtained the complete constitutive parameters of the material, which were verified by mechanical experiments with nonlinear strain paths. The effectiveness of different model combinations in predicting the plastic behavior and mechanical responses on medium-thickness high-strength steel plates is further evaluated.

Introduction

In the evolving landscape of material processing engineering, advanced stamped components offer a promising avenue for enhancing material efficiency and energy conservation. Particularly, the use of medium-thickness, high-strength steel plates, defined here as those exceeding 3 mm in thickness, represents a significant step forward in this domain [1]. These materials find extensive applications across various sectors, notably in the automotive industry, where they are integral to the structural integrity and functionality of commercial vehicle frames. Components such as rear mount lower brackets, longitudinal beams, cross beams, and filter mounts are pivotal examples showcasing the material's versatility and reliability.

Despite their apparent advantages and growing adoption, the metal forming processes of medium-thickness, high-strength steel plates encapsulate a series of complex phenomena that

distinctly set them apart from their thin sheet counterparts. The inherent challenges—plastic anisotropy, springback, non-uniform material flow, and fracture mechanisms—underscore a critical gap in our current understanding and predictive capabilities. The complicated behavior of these materials under forming conditions necessitates a comprehensive analytical framework that transcends conventional methodologies, thereby facilitating a deeper insight into their mechanical response and formability characteristics.

In addressing these challenges, the present study underscores a concerted effort to bridge the knowledge gap through the development of advanced elastic-plastic constitutive models, which are pivotal in simulating the plastic behavior of the medium-thickness steel with greater precision and fidelity. The integration of sophisticated while easily yield criterion—namely Hill 48 [2]—alongside the Armstrong-Frederick (A-F) kinematic hardening model [3], lays the groundwork for an innovative approach that marries theoretical rigor with practical applicability.

The choice of 5-mm-thick 750L high-strength steel as the focal point of this investigation is motivated by its widespread usage and representative nature within the context of medium-thickness applications. The intricacies associated with calibrating anisotropic yield criterion parameters, particularly along the thickness direction, pose a significant challenge that this study aims to surmount. By leveraging high-resolution full-field crystal plasticity (CP) simulations [4, 5], this study endeavors to extract material parameters that are otherwise elusive through conventional means. The subsequent calibration of kinematic hardening models via the inverse analysis method [6] further exemplifies the study's methodical approach to constitutive modeling.

This research culminates in a set of comprehensive constitutive parameters that embody the steel's intricate behavior under a spectrum of loading conditions. The validation of these models through a series of mechanical experiments, characterized by nonlinear strain paths, serves as a testament to their robustness and predictive accuracy.

The ensuing discourse is structured to provide an in-depth exploration of the aforementioned themes, beginning with a detailed exposition of the experimental details, multiscale constitutive, and CP modeling technique employed in this study. Subsequent sections will delve into the results and discussions, elucidating the empirical findings and theoretical implications that emerge from this research. Collectively, these insights aim to advance the field of material engineering, offering a detailed understanding of medium-thickness high-strength steel plate and paving the way for their optimized utilization in industrial applications.

Experiments and consititutive models

A series of experiments were meticulously designed to characterize the mechanical behavior and anisotropic properties of the medium-thickness high-strength steel plate. The material's stress-strain response and its plastic anisotropy are the key focal points of this investigation.

Uniaxial tensile testing. The uniaxial tensile tests were conducted using an Instron universal testing machine, complemented by the ARAMIS Digital Image Correlation (DIC) system for enhanced strain measurement accuracy, as shown in Fig. 1a. The tests targeted various material orientations to ascertain the anisotropy in mechanical properties. Specifically, samples were tested along three principal directions: transverse direction (TD), rolling direction (RD), and diagonal direction (DD, or 45° to the rolling direction). To ensure the robustness of the results, each direction was subjected to five replicate tests. Additionally, testing was expanded to include orientations of 22.5° and 62.5° to validate the yield criterion model's accuracy.

Sample dimensions for the tensile tests adhered to the GB/T 228.1-2021 (ISO6892-1:2019) standard for metallic material tensile testing at room temperature. The gauge length and width of the samples were set to 50mm and 12.5mm, respectively. Prior to testing, the thickness of each specimen was measured at three equidistant points along the gauge length, and the average value was adopted as the sample's thickness.

Compression testing. To complement the tensile data and capture the steel's mechanical behavior in the thickness direction, compression tests were performed on cubic specimens extracted from each plate, as shown in Fig. 1b. The dimensions for these specimens were 4 mm×4 mm×5 mm. Ensuring uniform contact and reducing friction between the specimens and the compression platens were crucial. This was achieved by grinding the sample's top and bottom surfaces and applying a thin layer of lubricant on the platens. The compression rate was standardized at 0.001/s, equating to 0.3mm/min, with the test concluding at a true strain of 0.2. The ARAMIS DIC system provided real-time strain readings throughout the compression tests.

Tensile-compression testing. To calibrate the kinematic hardening model for the steel, a series of tensile-compression experiments were conducted. The experimental campaign was structured in two sequential stages: tensile loading followed by unloading, and subsequent compression testing. This approach was employed for each material variant along both RD and TD. For each direction, the sample was subjected to three distinct pre-strain levels during the tensile loading stage, and each pre-strain level test was repeated three times. Subsequent to the tensile test, small rectangular specimens were extracted from the pre-strained sample for compression testing, as shown in Fig. 1c. The dimension of these samples was tailored to 8 mm×5 mm×5 mm. The compression was conducted at a rate of 0.5 mm/min, targeting a total deformation of ~20%.

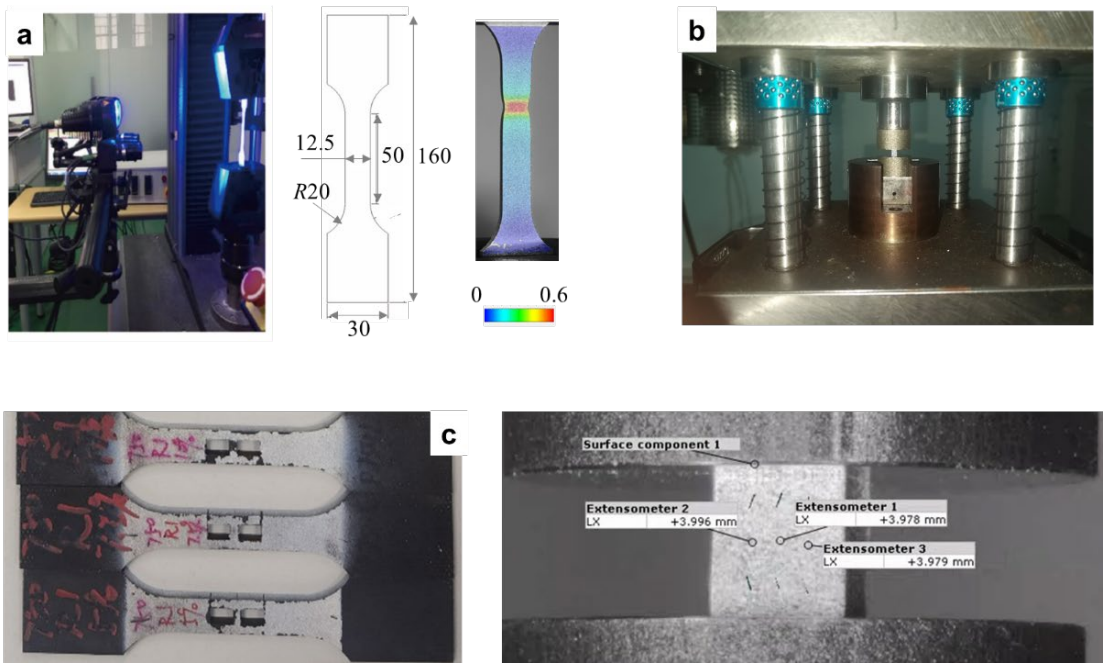

Fig. 1. The tensile test setup integrated with the DIC system, the geometric dimensions of the tensile specimens and the strain distribution contour of the specimen after necking. (b) The specialized apparatus for the compression test of the thick steel plate. (c) The pre-strained specimens for cyclic loading experiments, the sampling images for the sequential compressive test, and the schematic diagram of the reverse compression experiment.

Microstructure characterization. To understand the initial microstructural characteristic of the steel as well as get the data for building the microstructural representative volume element (RVE) for CP modeling, Electron backscatter diffraction (EBSD) experiments were used to characterize the steel's microstructure and texture. Samples measuring 6 mm×6 mm×5 mm were extracted from the as-received steel plate, with clear demarcations for the RD, TD, and ND. These samples were bisected to isolate surfaces for EBSD characterization, specifically choosing the RD-TD plane from both the surface and intermediate section of the plate.

The EBSD characterization was conducted using a NOVA NanoSEM 230 scanning electron microscope, with scanning voltage of 20 kV, beam size of 6, and working distance of 13 mm. The electron microscope operated at a magnification of 2000×, targeting an EBSD characterization area of 100 μm × 100 μm. The scan step size was determined to be 0.2 μm, resulting in a grid of 500 × 500. Fig. 2 shows the characterized microstructure of the as-received steel. The phases detected included ferrite (and martensite)—BCC phase and very little austenite and cementite, and the austenite and cementite constituents were ignored in the building of RVE.

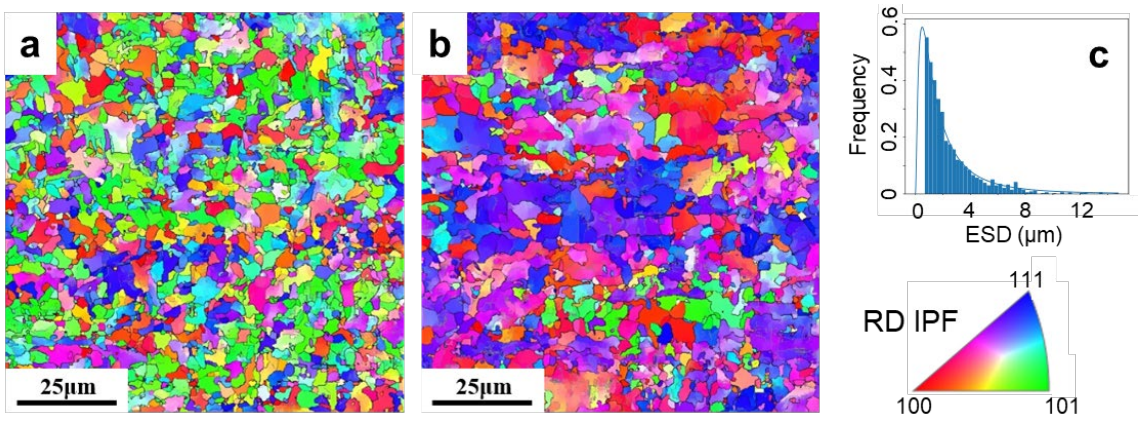

Fig. 2. The initial microstructure of the steel characterized by EBSD on the RD-TD surface (a) and RD-TD section at the half thickness (b). (c) The frequency distribution of grain size. The EBSD maps are colored with the RD inverset pole figure (IPF).

Multiscale material models

Hill 48 yield criterion. The Hill 48 yield criterion is foundational in the field of material science and engineering, particularly for characterizing the anisotropic behavior of metals during plastic deformation. The criterion extends the von Mises yield condition to accommodate anisotropic materials. The criterion is expressed as a quadratic function of the stress components, tailored to capture the anisotropy in different material directions. The general form of the Hill 48 criterion for orthotropic materials (common in rolled metal sheets) is:

$$\sqrt{F(\sigma_{22}-\sigma_{33})^2+G(\sigma_{33}-\sigma_{11})^2+H(\sigma_{11}-\sigma_{33})^2+2L\sigma_{23}^2+2M\sigma_{31}^2+2N\sigma_{12}^2} \quad (1)$$

Here, F, G, H, L, M, N are material constants that reflect the anisotropic properties of the material. These constants are typically determined experimentally, often through tensile tests in different directions relative to the material's microstructure.

The Armstrong-Frederick kinematic hardening model. The A-F kinematic hardening model is a well-regarded constitutive framework used to describe the behavior of materials undergoing cyclic loading and the Bauschinger effect. The fundamental idea behind the A-F model is to enhance the classical kinematic hardening rule by incorporating a nonlinear term that describes the evolution of the backstress α_{ij}, which is given by:

$$d\alpha_{ij} = \frac{2}{3}C d\varepsilon_{ij}^{p} - \gamma\, \alpha_{ij} d\bar{\varepsilon}^{p} \quad (2)$$

Here, $d\alpha_{ij}$ represents the increment in backstress, $d\varepsilon_{ij}^{p}$ is the increment in plastic strain, $d\bar{\varepsilon}^{p}$ is the equivalent plastic strain increment. C and γ are material constants; C controls the rate at which the backstress evolves with plastic deformation, and γ is a dynamic recovery parameter that dictates the rate at which the backstress is reduced as the material undergoes continued plastic deformation.

Crystal plasticity modelling. Determining material parameters for three-dimensional anisotropic yield criterion presents a significant challenge, particularly for the parameters related to the thickness direction anisotropy of metal sheet/plate. In recent years, virtual laboratory techniques based on CP have emerged as a powerful tool for identifying parameters of advanced yield criteria. The core approach involves using a calibrated CP model to simulate and predict the mechanical response of materials under arbitrary stress states. By generating a multitude of such stochastic stress points and employing optimization algorithms, material parameters of advanced yield criteria can be conveniently ascertained. It is imperative, however, that the CP and the microstructural RVE models are sufficiently accurate.

A finite strain rate-dependent CP model is employed in this study. The CP model adopts a simple power-law expression for the flow equation, which delineates the relationship between shear strain rate and resolved shear stress as follows,

$$\dot{\gamma}^{\alpha} = \dot{\gamma}_0 \left(\frac{|\tau^{\alpha}|}{g^{\alpha}}\right)^{\frac{1}{m}} \text{sign}(\tau^{\alpha}) \tag{3}$$

where $\dot{\gamma}^{\alpha}$ is the reference slip rate on the specific slip system, g^{α} represents the slip resistance of slip system α, and m is the strain rate sensitivity coefficient. g^{α} signifies the resistance against dislocation movement encountered during plastic deformation. A modified phenomenological model, incorporating the is adopted to describe evolution g^{α} as follows,

$$\dot{g}^{\alpha} = \begin{cases} 0, & \int \dot{\gamma}^{\alpha}\, dt < \gamma_L \\ \sum_{\beta=1}^{n} h_{\alpha\beta} \left|\dot{\gamma}^{\beta}\right|, & \int \dot{\gamma}^{\alpha}\, dt \geq \gamma_L \end{cases} \tag{4}$$

$$h_{\alpha\beta} = h_0 \left[q + (1-q)\delta^{\alpha\beta}\right] \left|1 - \frac{g^{\beta}}{g_s^{\alpha}}\right|^{a} \text{sign}\left(1 - \frac{g^{\beta}}{g_s^{\alpha}}\right) \tag{5}$$

where γ_L, h_0, g_s, and a are material constants representing the maximum shear strain before the vanish of Lüders straining, reference self-hardening modulus, saturation slip resistance, and hardening exponent, respectively; the initial CRSS is denoted as g_0. The parameter q denotes the ratio of interaction strengths among various slip systems, characterizing the distinction between self-hardening and latent hardening of slip system. More details about the adopted CP model can be refered to [4].

A pivotal element in conducting the CP simulation is the deployment of high-resolution RVE that capture the microstructural intricacies of the studied steel. In this work, the open-source modeling software DREAM.3D [7] was employed to construct a polycrystalline RVE model for the steel, leveraging the steel's EBSD data as a foundational input. The reconstructed RVE embodies the heterogeneity and anisotropy inherent in the steel's microstructure (grain size, morphology, and orientation obtained from EBSD data), serving as a critical foundation for subsequent CP simulations.

Results and Discussion

Fig. 3 presents the experimental results of the mechanical tests of the steel. The results indicate that the steel plate exhibits strong anisotropic mechanical behavior, as evidenced by the varying stress-strain curves and r values along different directions. The RD curve shows a continuous stress increase with strain, featuring a steep initial elastic region followed by a gradual transition into plastic deformation, indicating strain hardening. The TD curve is similar to RD, but with a slightly higher yield point and ultimate strength, which could be due to effect of strong crystallographic texture of the as-received steel, as shown in Fig. 2. The DD curve, represented by a dashed line, lies between RD and TD, suggesting that the mechanical properties in this direction are intermediate.

Moreover, the r value, a measure of the material's ability to resist thinning or thickening when stretched, varies with direction. The r value is highest along the RD, intermediate along DD, and lowest along TD. This difference in r values suggests that the steel plate is most ductile along the RD and least along TD, which can significantly affect sheet metal forming operation.

As previously mentioned, the EBSD data illustrated in Fig. 2 was used to construct the RVE necessary for CP simulations. The reconstructed high-resolution RVE presented in Fig 4a encompasses approximately 10,000 equiaxed grains, with grain size and orientation distributions derived from the EBSD data. Utilizing the established RVE and the stress-strain curves from Fig. 3 (RD and TD), a inverse analysis method was employed to determine the material parameters of the CP model, as detailed in Table 1. Fig. 4b displays a comparison between the flow stress curves predicted by the CP simulation and from the experiments. The simulated results correlated with the experimental data satisfactorily, affirming the calibrated CP model's adeptness in describing the steel's mechanical behavior along various orientations, inclusive of the Lüders stress plateau and work-hardening.

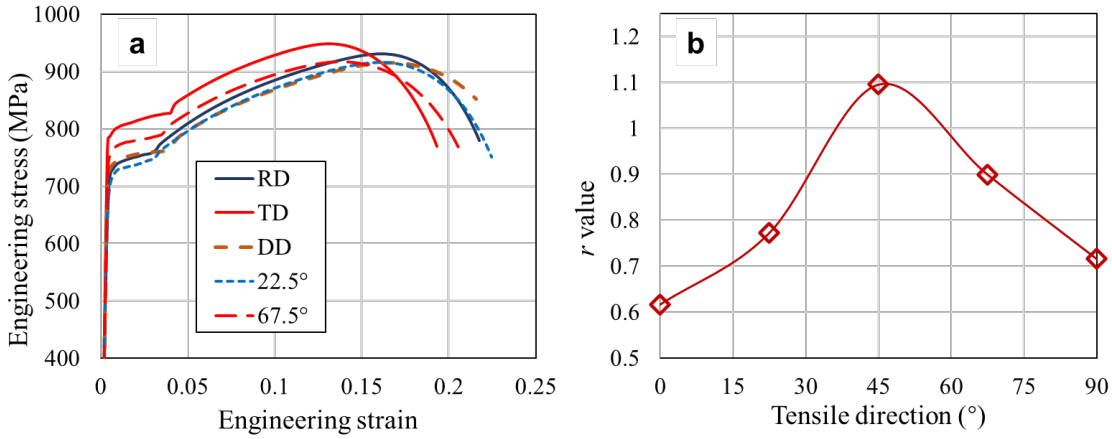

Fig. 3. Engineering stress-strain curves and r-values of the steel tensile tested along different directions.

Table 1. Materials parameters of the CP for the medium-thickness steel. The parameters were identified by the inverse analysis method.

Slip system	g_0^α/MPa	g_s^α/MPa	h_0/MPa	a	γ_L	$\dot{\gamma}_0$/s^{-1}	q	n
$\{\bar{1}10\}\langle 111\rangle$	300	435	825	1.04	0.0595	0.001	1.4	20
$\{\bar{2}11\}\langle 111\rangle$	319	449	2555	1.34				

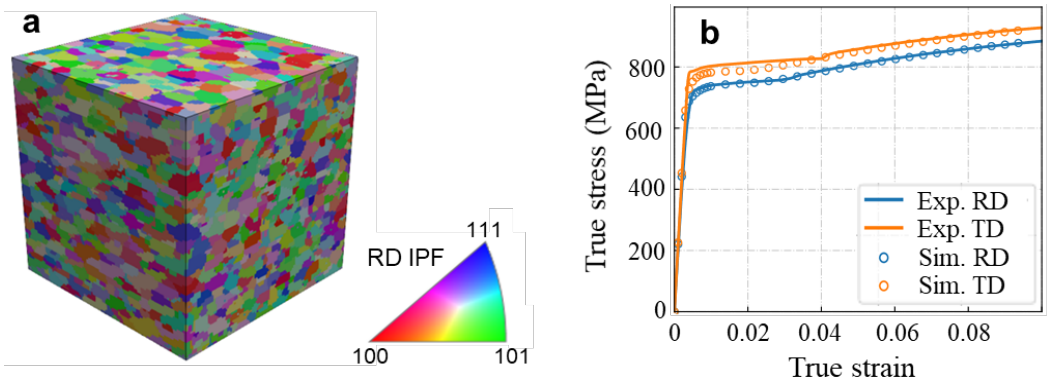

Fig. 4. (a) The RVE constructed from the EBSD data for CP simulations. (b) The comparison between the flow stress curves in RD and TD predicted by the calibrated CP simulation and from the experiments.

Building upon the previously calibrated CP model, we employed it as a virtual laboratory to conduct simulations under 100 random stress states. This approach yielded mechanical response data of the polycrystalline RVE under arbitrary stress conditions. Subsequently, we used these 100 stress data points and applied the Levenberg–Marquardt algorithm to fit the six material parameters of the Hill 48 yield criterion, as depicted in Table 2. Fig. 5 illustrates the yield loci predicted by the Hill 48 criterion along with the r values for different tensile directions. The results conspicuously demonstrate that the identified Hill 48 yield criterion adeptly characterizes the steel's anisotropic mechanical behavior and plastic flow.

Table 2. Materials parameters of Hill 48 yield criterion calibrated by the CP based virtual laboratory.

F	G	H	L	M	N
0.5329	0.6177	0.3823	1.9511	1.5949	1.8354

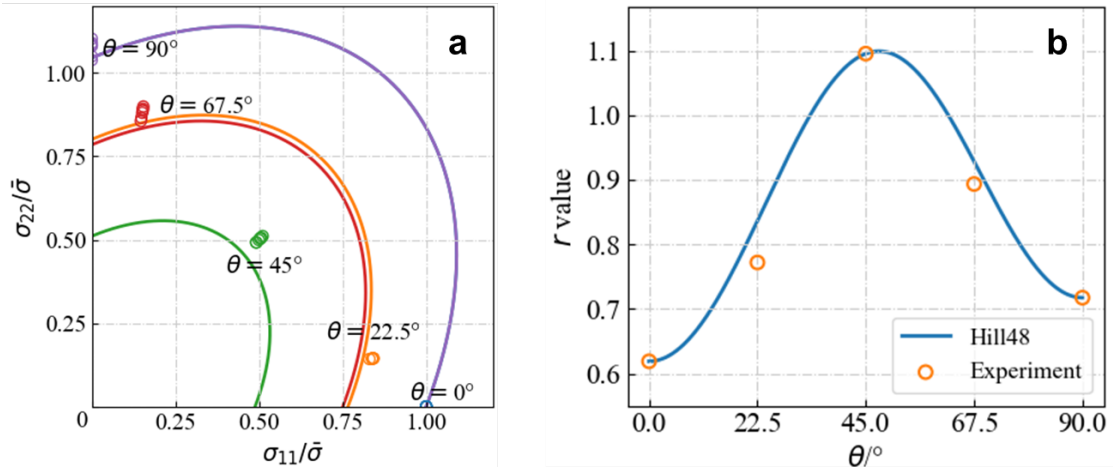

Fig. 5. (a) The comparison between the experimental yield loci (open symbols) and those predicted by the calibrated Hill 48 yield criterion. (b) The comparison between the experimental r values (open symbols) and those predicted by the calibrated Hill 48 yield criterion

We further integrated the calibrated Hill 48 yield criterion with the A-F kinematic hardening model and the Swift strain hardening model to develop a comprehensive three-dimensional elastic-plastic constitutive model tailored for the medium-thickness steel plate. Specifically, to address the Lüders yield plateau phenomenon exhibited by the steel, we modified the Swift model to accurately capture the Lüders plateau occurring during tensile deformation, as shown in Eq. 6.

$$\bar{\sigma} = \begin{cases} A(\bar{\varepsilon}^p + \varepsilon_0)^n + a(\bar{\varepsilon}^p - \varepsilon_b)^2 - a(\varepsilon_L - \varepsilon_b)^2 & \bar{\varepsilon}^p < \varepsilon_L \\ A(\bar{\varepsilon}^p + \varepsilon_0)^n & \bar{\varepsilon}^p > \varepsilon_L \end{cases} \quad (6)$$

The inverse analysis method combined with the particle swarm optimization algorithm were employed to identify the material parameters of this constitutive model, as shown in the Table 3. Fig. 6 presents the stress-strain curves of the steel under reverse loading following three different pre-strain levels in tension, including both experimental and simulated predictions. The results indicate a pronounced Bauschinger effect of the steel, and the established constitutive model adeptly describes the steel's work hardening, the Bauschinger effect upon reverse loading, and kinematic hardening behavior.

In summary, the elastic-plastic constitutive model established in this study, along with the material parameters calibrated using CP simulation and inverse analysis method, effectively characterizes the anisotropic behavior, mechanical behavior (including work hardening and the Lüders yield plateau), and kinematic hardening behavior of the medium-thickness steel plate.

Table 3. Materials parameters of the A-F kinematic hardening model and the Swift model for the steel. The parameters were identified by the inverse analysis method.

a/GPa	ε_b	ε_L	A/MPa	ε_0	n	C/GPa	γ
577	0.0216	0.0209	925	0.0118	0.212	64.2	219

Conclusions

This study focuses on medium-thickness high-strength steel plate widely applied in the automotive industry, examining their anisotropic mechanical behavior and Bauschinger effect through systematic mechanical testing. The steel exhibits pronounced anisotropic mechanical properties and plastic flow, the Luders yield plateau, and significant Bauschinger effect. We integrated the Hill 48 yield criterion, Armstrong-Frederick kinematic hardening model, and the Swift strain hardening model to develop a three-dimensional elastoplastic constitutive model tailored for the forming operation of medium-thickness steel plate. Utilizing high-resolution crystal plasticity simulations as a virtual laboratory, we employed inverse analysis to calibrate material parameters of the anisotropic yield criterion, and further determined the complete parameters for the constitutive model. The results demonstrate that the established constitutive model and its parameters accurately describes the complex mechanical behaviors and deformation characteristics of the medium-thickness steel plate.

The models and the multiscale modelling technique developed in this paper provide an essential reference for constitutive model development and numerical simulation of medium-thickness plates.

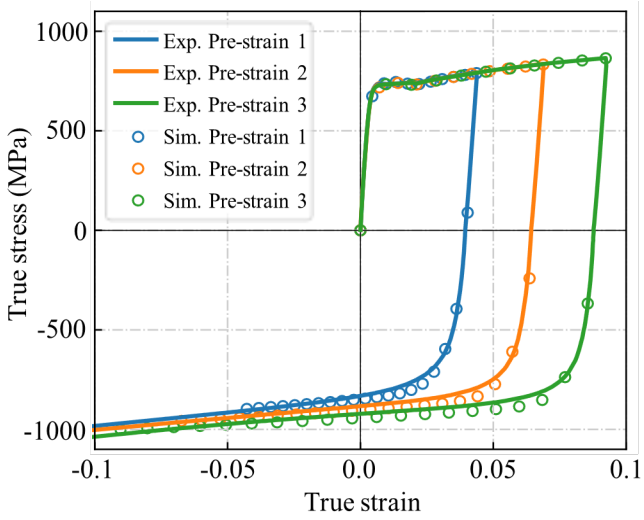

Fig. 6. Stress-strain curves for reverse loading following different pre-strain levels. The solid lines represent experimental data. Corresponding simulation results are depicted with open circles, aligning with their respective experimental curves. This comparison highlights the constitutive model's accuracy in capturing the mechanical response of the steel after varying degrees of pre-straining.

Acknowledge
Financial assistance of the National Natural Science Foundation of China (52075329) is acknowledged.

References

[1] C. Zhu, P. Gu, Y. Yu, Z. Tao, H. Zhang, Layered fracture prediction of QStE700 medium-thickness steel plate under tensile loading, Proceedings of the Institution of Mechanical Engineers, Part B: J. Eng. Manuf. 235 (2021)1144-1153. https://doi.org/10.1177/0954405420978035

[2] R. Hill, E. Orowan, A theory of the yielding and plastic flow of anisotropic metals, Proceedings of the Royal Society of London Series A Math. Phys. Sci. 193 (1948) 281-297. https://doi.org/doi:10.1098/rspa.1948.0045

[3] C.O. Frederick, P.J. Armstrong, A mathematical representation of the multiaxial Bauschinger effect, Mater. High Temp. 24 (2007) 1-26. http://dx.doi.org/10.3184/096034007X207589

[4] H. Zhang, M. Diehl, F. Roters, D. Raabe, A virtual laboratory using high resolution crystal plasticity simulations to determine the initial yield surface for sheet metal forming operations, Int. J. Plast. 80 (2016) 111-138. https://doi.org/10.1016/j.ijplas.2016.01.002

[5] A. Nascimento, S. Roongta, M. Diehl, I.J. Beyerlein, A machine learning model to predict yield surfaces from crystal plasticity simulations, Int. J. Plast. 161 (2023) 103507. https://doi.org/10.1016/j.ijplas.2022.103507

[6] H. Ma, Y. Li, H. Zhang, Q. Li, F. Chen, Z. Cui, A virtual laboratory based on full-field crystal plasticity simulation to characterize the multiscale mechanical properties of AHSS, Scientific Reports 12 (2022). https://doi.org/10.1038/s41598-022-09045-8

[7] M.A. Groeber, M.A. Jackson, DREAM.3D: A Digital Representation Environment for the Analysis of Microstructure in 3D, Integr. Mater. Manuf. Innov. 3 (2014) 56-72. https://doi.org/10.1186/2193-9772-3-5